Remote Sensing of Environment 158 (2015) 193–206

Contents lists available at ScienceDirect

Remote Sensing of Environment

journal homepage: www.elsevier.com/locate/rse

Mapping dynamic cover types in a large seasonally flooded wetland using extended principal component analysis and object-based classification

Iryna Dronova [a,b,*], Peng Gong [b,c,d,e,f], Lin Wang [c,d,e,g], Liheng Zhong [b]

[a] Department of Landscape Architecture & Environmental Planning, College of Environmental Design, University of California Berkeley, CA 94720-2000, USA
[b] Department of Environmental Science, Policy and Management, Division of Ecosystem Science, College of Natural Resources, University of California, Berkeley, CA 94720-3114, USA
[c] State Key Laboratory of Remote Sensing Science jointly sponsored by the Institute of Remote Sensing Applications of Chinese Academy of Sciences and Beijing Normal University, Beijing 100101, China
[d] Center for Earth System Science, Tsinghua University, Beijing 100084, China
[e] Poyang Lake Ecological Research Station for Environment and Health, Duchang, 332600, China
[f] Joint Center for Global Change Studies, Beijing 100875, China
[g] Chinese Academy of Fishery Sciences, Beijing 100141, China

ARTICLE INFO

Article history:
Received 25 August 2012
Received in revised form 15 October 2014
Accepted 29 October 2014
Available online 5 December 2014

Keywords:
Dynamic cover types
Wetland remote sensing
Object-based image analysis
PR China
Extended PCA
Phenology
Change trajectory analysis

ABSTRACT

Periodically inundated wetlands with high short-term surface variation require special approaches to assess their composition and long-term change. To circumvent high uncertainty in single-date analyses of such areas, we propose to characterize them as dynamic cover types (DCTs), or sequences of wetland states and transitions informed by physically and ecologically plausible surface processes. This study delineated DCTs for one 2007–2008 flood cycle at Poyang Lake, the largest freshwater wetland in China, using spatial and temporal orientation modes of extended principal components analysis (EPCA) and supervised object-based classification of multi-spectral and radar image series. Classification accuracy was compared among three sets of attributes selected by machine-learning optimization from object-level mean and standard deviations of: 1) image time series alone; 2) the most informative EPCA outputs alone and 3) image time series and EPCA results together. Classification uncertainty was additionally assessed as low values of object's maximum class membership (<0.5). The highest accuracy was achieved with a larger set of 33 attributes selected from combined time series and EPCA results (overall accuracy 95.0%, kappa 0.94); however, accuracies with smaller sets of variables from input image series or EPCA results alone were comparably high (93.1% and 94.7%, respectively). All three selected attribute sets included standard deviations of image and/or EPCA values, suggesting the utility of object texture in dynamic class discrimination. The highest classification uncertainty was observed primarily along the mapped class boundaries, in some cases indicating minor change trajectories for which prior reference data were not available. Results indicate that DCTs provide a reasonable classification framework for complex and variable Poyang Lake wetlands that can be facilitated by EPCA transformation of complementary remote sensing time series. Future work should test this approach over multiple change cycles and assess sensitivity of results to temporal frequency of input image series, alternative variable selection algorithms and other remote sensors.

1. Introduction

Landscape ecosystems are never truly static; they constantly vary due to physical processes, biological interactions, phenology and disturbance. For a given ecosystem property, the assumption of "change" versus "no change" over a time frame of interest is important for understanding long-term resilience and response to natural and anthropogenic change drivers (Foley et al., 2005; Liu & Cai, 2011; Neuenschwander & Crews, 2008). Remote sensing platforms greatly facilitate studies of landscape change by providing repeated monitoring over large areas and locations with difficult ground access (Gong et al., 2010; Ordoyne & Friedl, 2008; Ozesmi & Bauer, 2002; Rebelo, Finlayson and Nagabhatla, 2009). However, the accuracy of detection and interpretation of change may be constrained by spatial resolution, extent and acquisition frequency of the data (Assendorp, 2010; Coppin, Jonckheere, Nackaerts, Muys and Lambin, 2004; Liu & Cai, 2011; Lunetta, Johnson, Lyon and Crotwell, 2004), and by the short-term variation of land surface properties (Crews-Meyer, 2008; Dronova, Gong and Wang, 2011; McCleary, Crews-Meyer and Young, 2008).

Traditional mapping approaches have often focused on static classes representing discrete states of surface cover observable for extended periods of time. The "change" is assumed to occur for a given location if the highest-probability cover classes differ among successive points in time, and various change detection techniques have been summarized in several reviews (Coppin et al., 2004; Gong & Xu, 2003; Lu, Mausel, Brondizio and Moran, 2004; Mas, 1999). However, both

* Corresponding authorat: 202 Wurster Hall # 2000, Department of Landscape Architecture & Environmental Planning, College of Environmental Design, University of California Berkeley, CA 94720-2000, USA.
E-mail address: idronova@berkeley.edu (I. Dronova).

http://dx.doi.org/10.1016/j.rse.2014.10.027
0034-4257/

classification and change detection are challenging in rapidly varying areas such as periodically inundated wetlands, where short-term surface dynamics produce transitional states and fine-scale mixtures of classes and may obscure long-term surface trends. Notably, such complex landscapes often support unique ecological services and high biological diversity (Dudgeon et al., 2006; Gibbs, 2000; Ordoyne & Friedl, 2008; Wang et al., 2012) and thus call for alternative approaches to characterize them in order to assess their response to climate change and human activities.

Several strategies to characterize highly variable landscapes were offered by previous research. One of them defines classes as static cover types prevalent over the whole time range of the data but classified based on their multi-temporal signatures, such as in studies of crop dynamics (Zhong, Hawkins, Biging and Gong, 2011) and in the National Dynamic Land Cover Dataset for Australia (Lymburner et al., 2011). This approach reveals class-specific phenological spectral trajectories (Wang et al., 2012; Zhong et al., 2011) and early signals of potential state shifts (Lymburner et al., 2011); however, "single class representation of dynamic behavior" (Lymburner et al., 2011) may prohibit detection of the actual changes between classes (Sun, Zhao, Gong, Ma and Dai, 2014).

With the second strategy, land-cover change pathways are derived from multi-date images (Lawrence & Ripple, 1999; Liu & Cai, 2011; Mertens & Lambin, 2000; Vågen, 2006) as multi-temporal transition classes (Hess, Melack, Novo, Barbosa and Gastil, 2003) or as the outputs of multi-date image series transformations with principal component analysis (PCA), Kauth–Thomas algorithm and other methods (Byrne, Crapper and Mayo, 1980; Collins & Woodcock, 1996; Coppin, Nackaerts, Queen and Brewer, 2001; Ribed & Lopez, 1995; Seto et al., 2002b). A promising but under-explored strategy is using different forms of PCA to highlight recurring temporal patterns in space (S-mode PCA), prevalent spatial patterns over time (T-mode) (Cattell & Murphy, 1973; Richman, 1986), or shared temporal and spatial patterns among different datasets (extended PCA, or EPCA; Neeti & Eastman, 2014).

The third type of studies aims to distinguish longer-term changes from short-term variation caused by phenology or disturbance. Such analysis may be implemented by comparing inter- and intra-annual land cover changes as a panel approach described by Crews-Meyer (2008) and McCleary, Crews-Meyer and Young (2008), or by fitting regression to long-term data series and analyzing residuals for signals of non-recurring disturbance and unusual events (Neuenschwander & Crews, 2008).

While all these approaches offer useful strategies for complex landscapes such as periodically flooded wetlands, they also highlight an important challenge. Complex surface composition and dynamics may result in a large number of detected unique change pathways, some of which may not be physically plausible (Hess et al., 2003; Liu & Cai, 2011; Villa, Boschetti, Morse and Politte, 2012), representing error and noise (McCleary et al., 2008). This issue may be addressed by using ancillary information in class definition, transforming the images to highlight relevant patterns (Neeti & Eastman, 2014) and by reducing pixel-level local heterogeneity using primitive objects as mapping units (Chen, Hay, Carvalho and Wulder, 2012). In dynamic landscapes, periodic processes often produce regimes of change, sometimes along the gradients of change drivers such as inundation (Assendorp, 2010; Lenssen, Menting, van der Putten and Blom, 1999). These regimes may shape unique ecosystem types, functions and species assemblages and thus may be useful in landscape management, planning and conservation (Parrott & Meyer, 2012; Watson, Luck, Spooner and Watson, 2014). We will refer to these regimes as "dynamic cover types" (DCTs), or distinct sequences of wetland cover states and transitions observed within a given period of change cycle.

Delineation of dynamic classes may benefit from data transformations that accentuate both prevalent types of surface cover and key transitions — such as extended PCA searching for patterns recurring in both space and time (Cattell & Murphy, 1973; Neeti & Eastman, 2014; Richman, 1986). It may be also useful to map DCTs with object-based image analysis (OBIA) where prior to classification, image pixels are segmented into "objects" matching spatial entities (Blaschke, Lang, Lorup, Strobl and Zeil, 2000; Dronova et al., 2011, 2012; Lyons, Phinn and Roelfsema, 2012). Even small "primitive" objects have been shown to improve classification accuracy relative to pixels by smoothing local noise and enhancing class contrasts with non-spectral attributes (Conchedda, Durieux and Mayaux, 2008; Grenier et al., 2007; Kim, Warner, Madden and Atkinson, 2011; Lyons et al., 2012). Using prior knowledge to define DCTs may facilitate differentiating among long-term change and short-term variation for the processes of interest, while novel change or sporadic disturbances can be detected as deviations from DCT trajectories.

Our study aimed to delineate DCTs as major trajectories of annual wetland change cycle at Poyang Lake, the largest freshwater lake-wetland complex in China (Fig. 1). Dynamics of monsoon-driven inundation (Andreoli et al., 2007; Qi et al., 2009), vegetation phenology (Wang et al., 2012) and disturbance affect important ecological properties of this wetland, such as nutrient and greenhouse gas fluxes (Liu, Xu, Lin and Zhang, 2013), habitat for migratory waterbirds including critically endangered species (Barzen, Engels, Burnham, Harris and Wu, 2009) and life cycle of the snail species *Oncomelania hupensis*, the intermediate host to the parasite *Schistosoma japonica* causing severe human disease in the region and globally (Seto et al., 2002a). While "characteristic" dynamics of Poyang Lake's surface are still insufficiently understood (Feng et al., 2012; Sun et al., 2014), they are likely to change in the near future due to hydrological effects of the Three Gorges Dam upstream Yangtze River and local dams (Barzen et al., 2009; Finlayson, Harris, McCartney, Young and Chen, 2010; Guo, Hu, Zhang and Feng, 2012). Remote sensing classifications of this area from single-date images exhibit high uncertainty due to complex wetland cover and frequent transitional mixtures of classes (Dronova et al., 2011). These issues call for new strategies to address spatial and temporal complexity of this unique wetland ecosystem in order to improve the capacity for monitoring and, ultimately, landscape-level modeling of its change.

We focused on one flood cycle from summer 2007 to spring 2008 and seven dominant DCTs representing changes in water coverage, surface composition and plant phenology informed by previous research (Barzen et al., 2009; De Leeuw et al., 2006; Dronova et al., 2011, 2012; Qi et al., 2009; Wang et al., 2012). Our specific objectives were to 1) determine whether ecologically informed Poyang Lake DCTs could be distinguished with multi-temporal multi-spectral and microwave radar satellite images; and 2) assess the utility of S- and T-mode EPCA to highlight prevalent wetland cover states and key transitions (Cattell & Murphy, 1973; Neeti & Eastman, 2014; Richman, 1986) to facilitate DCT mapping from these different data types. Given spatial complexity of Poyang Lake's surface, we mapped DCTs by supervised classification of primitive image objects derived by multiresolution segmentation of the multi-date images. We further assessed the accuracy of DCT classifications with different sets of discriminating variables based on the image time series and EPCA outputs, assessed the uncertainty in class membership and discussed the strategies to enhance DCT analyses and extend them to multi-temporal framework in the future.

2. Methods

Our analysis was organized as follows (Fig. 2): we first performed the T- and S-mode EPCA transformation of the input remote sensing data and examined which spatial and temporal patterns in EPCA results corresponded to DCTs (Table 1). We then segmented the input image series into primitive objects and assigned training and test reference samples for DCT mapping using field data and high-resolution imagery. The statistics of training objects were examined to determine DCT class differences in 1) temporal trajectories calculated from the input image series; and 2) EPCA component (T-mode) and loading (S-mode) images. Next, we performed supervised object-based classification of DCTs followed by assessments of classification accuracy and uncertainty.

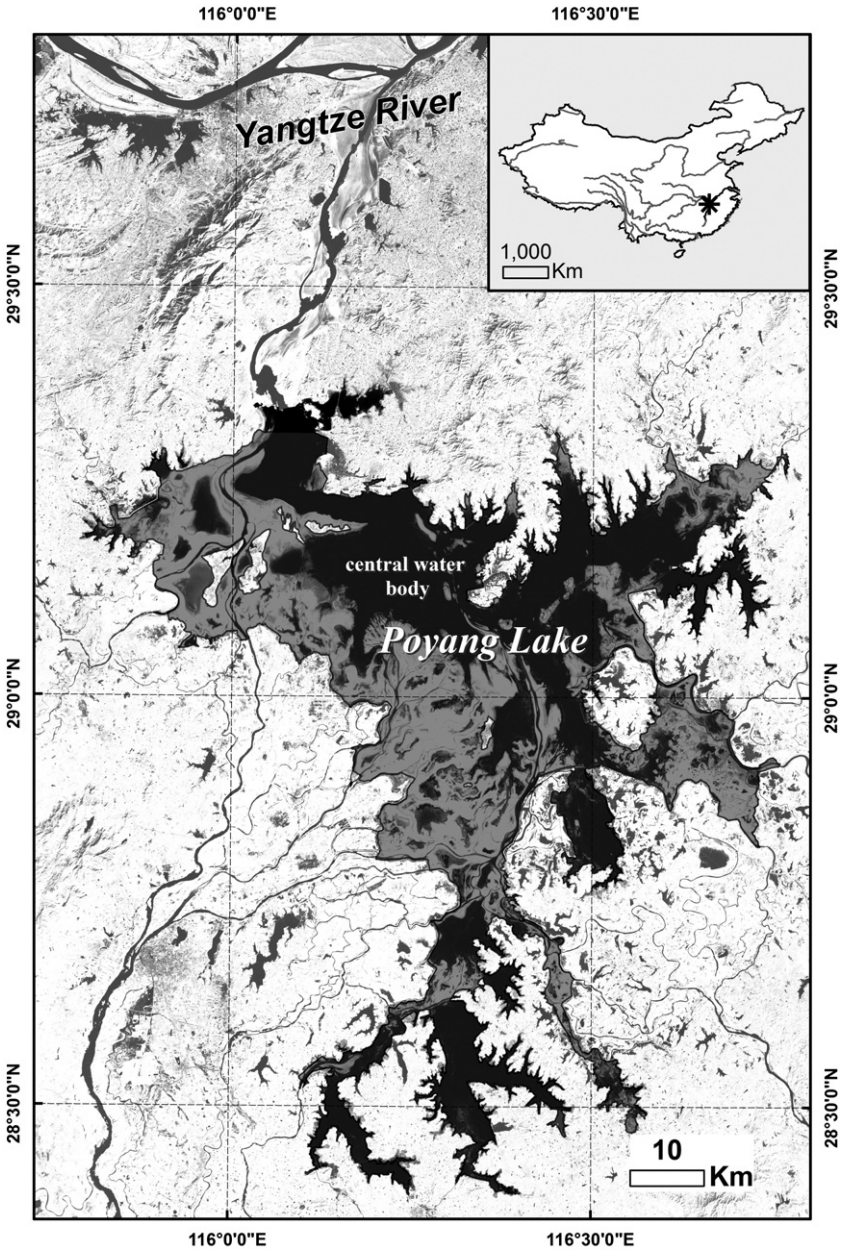

Fig. 1. Map of the study area in south-central portion of Poyang Lake, Jiangxi Province, People's Republic of China. Within the black outline boundary, dark-colored areas indicate permanent water bodies and central wetland area with long annual submersion period, and medium-gray areas indicate peripheral wetland zones with longer flood-free time.

2.1. Study area and wetland DCTs

This study focused on the main extent of Poyang Lake area (~3500 km^2) south from the channel with the Yangtze River (28°25′–29°20′N, 115°48′–116°44′E; Fig. 1). During the April-September rain season lake water coverage may exceed 4000 km^2; this period is also a "warm" growing season for aquatic vegetation and high-elevation grasses (Wang et al., 2012). From October to April the study area exhibits flood recession reaching the lowest water levels and spatial extent around January; at this time the exposed lake mudflats are gradually colonized by emergent vegetation of the "cool" growing season (Chen, Su, Fang and Chen, 2007; Dronova et al., 2011; Wang et al., 2012). Incremental water expansion and recession form contiguous landscape "zones" of similar annual submersion times at Poyang Lake (Andreoli et al., 2007; Feng et al., 2012; Hui, Xu, Huang, Yu and Gong, 2008; Zhao, Stein and Chen, 2011). Common wetland cover types observed within these zones as either extensive patches or fine-scale local mixtures can be broadly described as live or dead vegetation, water, sand and mudflats (Dronova et al., 2011).

We defined seven DCTs (Table 1) as sequences of wetland cover states recognizable at 32-m spatial resolution of remote sensing data and relevant to major surface features affecting ecosystem productivity, greenhouse gas fluxes and habitat of waterbirds and snails, based on previous studies (Barzen et al., 2009; Chen et al., 2007; De Leeuw et al., 2006; Dronova et al., 2011; Dronova et al., 2012; Guan, Lin, Zhou and Zeng, 2008; Liu, 2009; Liu et al., 2013; Wang et al., 2012; Zeng, Liu, Liu and de Leeuw, 2007). Two classes represented seasonally flooded grasslands: areas exposed by water in early fall and colonized by C3 plants (C3G), mainly *Carex* spp. with the highest biomass in late spring, and mixed C4–C3 grasslands (C4C3G) in higher-elevation lake periphery with *Miscanthus*, *Cynodon*, and *Arundinella* spp., usually green from spring to fall and senescent in winter (Guan et al., 2008; Wang et al., 2012; Zeng et al., 2007). Two DCTs represented "wetter" ephemeral mudflats exposed in the fall and re-flooded in spring, one

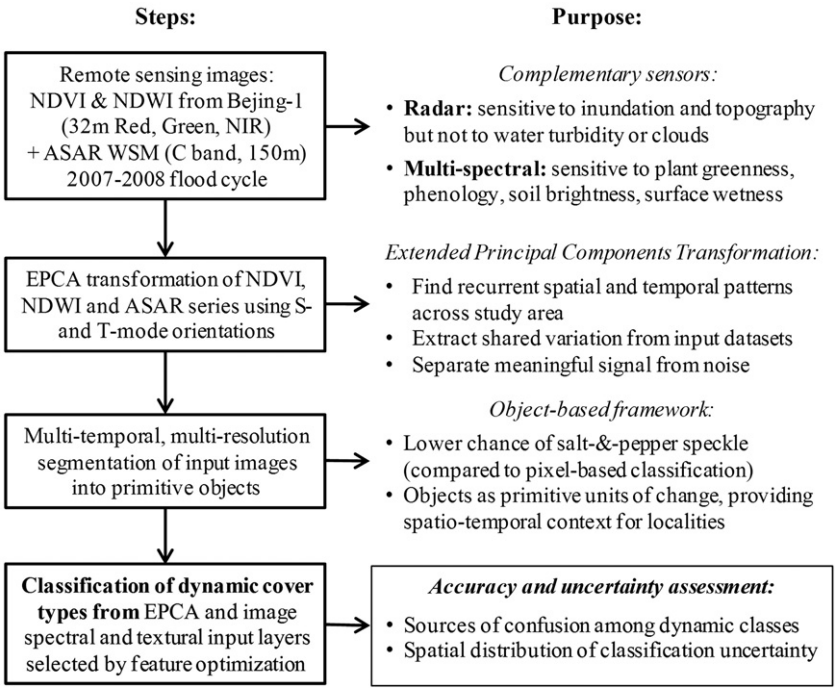

Fig. 2. Conceptual diagram of the major steps in dynamic cover type classification and analysis.

class with short flood-free period and no dense plant cover (EMN) and the other with ephemeral vegetation in winter (EMV). The remaining classes were permanent sand dunes (PS), permanent water bodies with no or warm season-only aquatic vegetation (PW; Table 2) and permanent water with aquatic macrophytes in late fall–winter (WAM).

2.2. Remote sensing data

We used remote sensing data from July–August 2007 to May 2008 (Table 2) covering the highest stage of summer flood of 2007, its subsequent recession, and the low water season until the new flooding of late spring 2008. The images included seven scenes of Beijing-1 microsatellite (32-m spatial resolution, near-infrared (NIR), red and green multi-spectral bands, 600-km swath and 5-day revisit time), and seven scenes of the ENVISAT Advanced synthetic Aperture Radar (ASAR) with C-band (5.3 GHz) in wide swath mode (WSM, 400-km swath) with single polarization (either HH or VV, Table 1), 150-m spatial resolution and 16–43° view angle range. Beijing-1 images were selected as the primary dataset because of spectral sensitivity to both hydrological landscape features and differences in composition and phenology of vegetation (Wang et al., 2012). Radar images were used as ancillary data to facilitate discrimination of highly turbid water and

Table 1
Major hypothesized dynamic cover types (DCTs) for Poyang Lake area for summer 2007–spring 2008 flooding period.

Dynamic cover type class	Sequence of states per flood cycle	Description
EMN — ephemeral mudflats, non-vegetated	Water → mudflat/sand → water	Portions of lake bottomland that are flood-free for a brief period near the minimum water levels in mid-winter; in the spring again become water or aquatic vegetation.
EMV — ephemeral mudflats, vegetated	Water → mudflat/sand → green emergent vegetation → water	Portions of lake bottomland that are exposed from flooding in late fall, become colonized by vegetation but then are flooded again in early-mid spring due to close proximity to flood source.
C3G — emergent C3 grassland, flooded	Water → mudflat/sand → green emergent vegetation	Portions of lake bottomland in higher-elevation areas surrounding smaller sub-lakes that are exposed from flood early enough for green C3 vegetation to develop and persist till the next flooding. Their main difference from EMV is in earlier exposure in the fall and later inundation in spring which leads to longer persistence of green vegetation.
C4C3G — mixed C-C3 grassland, partially flooded	[Water][a] → green vegetation → senescent or grazed vegetation → green emergent vegetation	Perennial vegetation on high-elevation lake periphery and ridges with short annual submersion times. Depending on location, plant composition may include C4 and C3 reeds or short C4 grasses that are often senescent in winter but green from early spring till late fall. May be disturbed by reed harvesting and burning of the stubble.
WAM — winter aquatic macrophytes	Water → aquatic vegetation → water	Permanent water with extensive aquatic vegetation beds primarily during the cool winter growing season.
PW — permanent water	Water all year round, occasionally with aquatic vegetation from late spring to mid-fall	Areas permanently covered with water within a given flood season. Water color and optical properties may change due to varying sediment content, and aquatic vegetation may influence its reflectance from late spring to early fall.
PS — permanent sand	Non-inundated sand features	High elevation sand hills and dunes in north-central part of the study area that are flood-free even at maximum flood stage.

[a] Some high-elevation ridges supporting C4 grasses and C3 reeds may remain flood-free in a given year (field observation).

Table 2
Satellite remote sensing images used in the dynamic cover type classification.

Satellite	Date	Flood cycle stage and wetland phenology
Beijing-1 (32 m; NIR, Red, Green)	Aug 16, 2007	Water coverage near annual maximum, only high-elevation ridges and permanent sand features are exposed
	Oct 17, 2007	Flood recession, C4 grasses at high biomass, C3 grasses emerge on newly exposed lake bottomland and mudflats
	Nov 30, 2007	Progression of the cool growing season with C3 grasses as the dominant green vegetation
	Jan 1, 2008	Progression of the cool growing season with abundant C3 grasses, C4 grasses mostly senescent and water levels near annual minimum with exposed adjacent mudflats
	Feb 16, 2008	Progression of the cool growing season with a short-term flooding event due to winter precipitation and snowmelt
	Mar 2, 2008	Emergent vegetation develops at warmer temperatures. Water levels very slowly begin to rise
	May 12, 2008	Early stage of the rain season, emergent vegetation near peak biomass
ASAR WSM (150 m, C-band), polarization is given for each image date	July 31, 2007 (VV)	Water coverage near annual maximum, only high-elevation ridges and permanent sand features are exposed
	Oct 28, 2007 (VV)	Flood recession, C4 grasses at high biomass, C3 grasses rapidly emerge on newly exposed mudflats
	Dec 18, 2007 (HH)	Progression of the cool growing season with C3 grasses as dominant green vegetation
	Jan 3, 2008 (HH)	Progression of the cool growing season with abundant C3 grasses, C4 grasses mostly senescent and water levels near annual minimum with exposed adjacent mudflats
	February 2, 2008 (HH)	Progression of the cool growing season with a short-term flooding event due to winter precipitation
	Apr 1, 2008 (HH)	Water levels begin to rise slowly, emergent vegetation approaching peak biomass
	April 20, 2008 (HH)	Water levels are rising, emergent vegetation near peak biomass

wet mudflats (Dronova et al., 2011) and of submersed and emergent wetland vegetation, because no accurate digital elevation and bathymetric data were available for the study area.

Beijing-1 sensor does not have the calibration onboard, and thus we used raw digital numbers (DNs) in the analysis. Beijing-1 images were radiometrically calibrated to Jan 01, 2008 scene using empirical linear relationships derived from pseudo-invariant targets of bright permanent sand on high-elevation dunes and dark permanent water reservoirs near cities. Calibrated images were converted into single-date layers of Normalized Difference Vegetation Index (NDVI, normalized difference of NIR and red bands) and Normalized Difference Water index (NDWI, McFeeters, 1996; normalized difference of green and NIR bands). The ASAR data were preprocessed by the State Key Laboratory of Remote Sensing Science, Beijing, China by converting raw data to backscatter coefficient values in Basic ENVISAT SAR Toolbox v. 4.2.1-a, correcting those for systematic variation using permanent-scatter urban features and radiometrically calibrating the images using pseudo-invariant targets. Radar images were resampled to Beijing-1 32-m resolution using nearest neighbor method in ENVI 5.0 (Exelis VIS Inc.).

2.3. Extended principal components analysis

To examine prevalent wetland cover states and transitions and to reduce the effects of image noise in classification, we decomposed three time series of NDVI, NDWI and ASAR into extended principal components using EPCA tool in Earth Trends Modeler, Idrisi Selva software (Clark Labs Inc.). Extended PCA is a type of spectral decomposition similar to regular PCA that examines patterns of shared variation among multiple time series datasets in space and/or in time (Neeti & Eastman, 2014). We chose this approach because some redundancy was expected in patterns of greenness, wetness and surface backscatter from NDVI, NDWI and ASAR series observing the same change phenomena. We performed standardized EPCA on these three time series using spatial (S-mode) and temporal (T-mode) forms of PCA orientation (Machado-Machado, Neeti, Eastman and Chen, 2011; Neeti & Eastman, 2014). The T-mode analysis highlights dominant spatial patterns over time; it outputs principal components as images for each series and a single set of loadings corresponding to input dates. The S-mode reveals recurrent temporal patterns over the study area, i.e. it searches for prevalent temporal trajectories among stacked "multi-temporal" pixels and outputs loadings as images for each input series and a single set of principal components as prevailing temporal profiles. By definition, the S-mode extended components were expected to highlight the dominant temporal change profiles in the study landscape, and therefore were of particular interest for potentially detecting trajectories of specific DCTs.

2.4. Image segmentation

To classify Poyang Lake DCTs, we used OBIA to avoid the salt-and-pepper speckle common in pixel classifications of wetlands and to enhance class contrast due to smoothing of local noise within objects (Dronova et al., 2012; Kim et al., 2011). The first step in the object-based analysis was segmentation of multi-temporal data into primitive objects as minimum mapping units with multiresolution segmentation tool in eCognition Developer 8.8 software (Trimble Inc). Multiresolution segmentation allows for flexibility in output object sizes (Baatz & Schäpe, 2000); however, its key parameters of scale, shape and compactness are often determined by trial-and-error and still rarely with quantitative approaches. Because for DCTs characteristic class objects were not known a priori, we first tested how scale, compactness and shape affected two scene-average metrics of object heterogeneity: within-object standard deviation and mean absolute spectral difference to neighbors, to select the optimal parameters (Dronova et al., 2011).

Specifically, we used seven NDVI layers as equally weighted segmentation inputs and calculated object heterogeneity metrics from February 2008 NDVI reflecting patchiness of the landscape at the low water season. Due to high variety of wetland patch sizes and shapes, the purpose of segmentation was not to immediately delineate all of the patches but rather to generate small object primitives as classification units while reducing local noise. Both metrics of heterogeneity increased with segmentation scale at all tested shape and compactness values. The rate of increase was the highest between scale values of 2 and 10, slowing and stabilizing after scale value of 11, which was selected as primitive object scale in our analysis. At scale 11, the lowest scene-average within-object standard deviation (indicating higher mean homogeneity) corresponded to shape and compactness values of 0.1 each that were used in the final segmentation. Primitive objects generated with these parameters from NDVI series were assumed to be invariant mapping units of DCTs over one annual cycle of wetland dynamics in our data. Prior to classification we isolated several residential and actively managed human land use areas that were not expected to follow "natural" wetland dynamics using Microsoft Bing image in ArcGIS 10 (ESRI Inc.).

2.5. Training sample statistics and supervised classification

From the segmentation output we selected 720 reference objects for subsequent classification based on several data sources. Ground surveys of wetland cover and vegetation along geolocated field transects were carried out in March-April and December 2007, January and April 2008, May 2010, November 2010 and January and March 2011 (Dronova et al., 2011, 2012; Wang et al., 2012), covering C3 and mixed C4-C3 grasslands, mudflats, permanent water and sand. For classes representing inaccessible ephemeral mudflats and winter aquatic vegetation, reference objects were assigned using visual comparison of multi-date images with high-resolution data from DigitalGlobe Worldview-1 and QuickBird sensors for May, September, November and December 2007 and January 2008, provided by the National Aeronautics and Space Administration (NASA) and The National Geospatial-Intelligence Agency (NGA) NextView program (cad4nasa.gsfc.nasa.gov). The reference set was randomly divided into 360 training and 360 test objects, each including 60 objects for spatially extensive PW and C3G classes, 50 objects for C3C4G, EPH, EMN and WAM and 40 objects for PS features with small spatial extent limited to one portion of the study area. We further examined differences in spectral-temporal trajectories of DCT class means of training objects with the untransformed NDVI, NDWI and backscatter series. We also tested which class pairs significantly differed ($p < 0.05$) in their object spectral (mean) and textural (standard deviation) values of EPCA T-mode component and S-mode loadings. This comparison was performed as one-way analysis of variance with post-hoc Scheffé's test (appropriate for unequal sample sizes and more conservative than other popular post hoc tests).

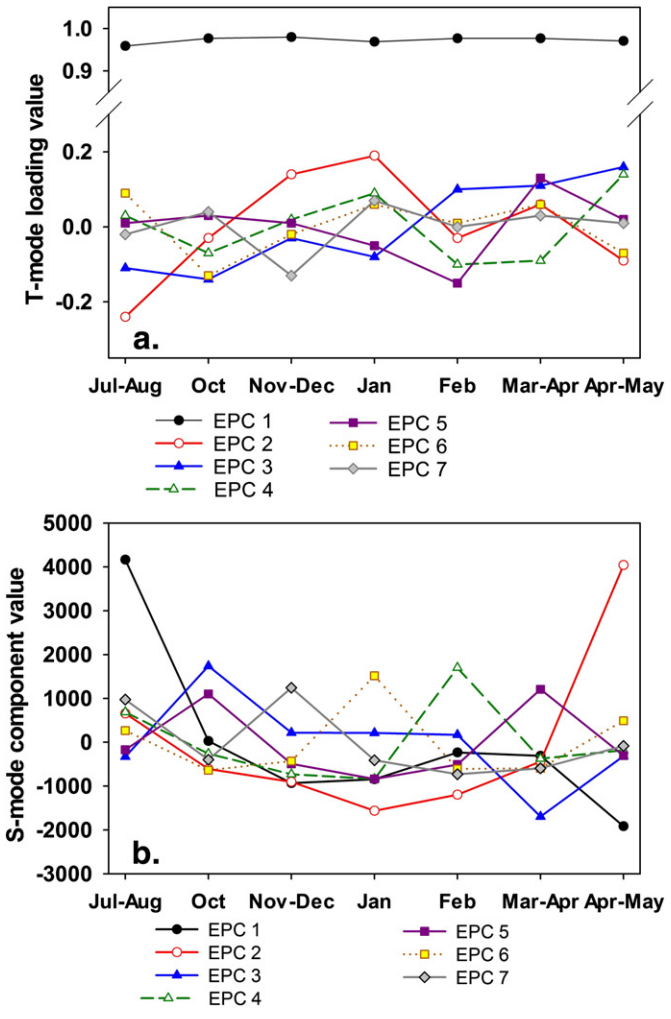

Fig. 3. Coefficients of the EPCA transformation of Beijing-1 NDVI and NDWI and ENVISAT ASAR backscatter series for Poyang Lake's 2007–spring 2008 flood period: a) loadings of T-mode orientation describing relative contributions of different image dates and b) S-mode component values as spatially prevalent temporal profiles.

We then conducted DCT classification in eCognition 8.8 using "Classification" tool which first evaluates class membership functions from the attribute values of training objects and then applies them to attributes of the unclassified objects to assign those to their respective highest-membership classes (ECognition Developer 8 Reference Book. V.8.8., 2012). This method requires specifying a set of class-discriminating attributes a priori from a potentially large number of various object variables. In our study these included object-level mean pixel values of the input NDVI, NDWI and backscatter images, the images of principal components (T-mode EPCA), component loading images (S-mode EPCA), object-level standard deviations of these datasets as simple indicators of object texture and two additional features representing temporal mean and temporal standard deviation of each object's NDVI values from the original series. To optimize the pool of discriminating variables for classification, we performed machine-learning attribute selection in Weka 3.6.9 data mining software (http://www.cs.waikato.ac.nz/ml/weka/; Hall et al., 2009). We used Weka's algorithm 'CfsSubsetEval' which considers predictive ability of individual variables in the subset together with the redundancy among them, coupled with the bi-directional 'BestFirst' search algorithm based on greedy hillclimbing local search (Hall, 1999). Attributes were selected separately from three data combinations: 1) using only the inputs of EPCA transformations, 2) using only the attributes from original series of NDVI, NDWI and backscatter and 3) using combined inputs from EPCA results and three image time series. Each selected subset of variables was separately applied to evaluate class membership functions with the slope of 0.1 (ECognition Developer 8 Reference Book. V.8.8., 2012) and classify unlabeled objects into DCTs. From each result, we calculated overall and class-specific accuracy metrics using contingency tables for the independent test object set. We also assessed spatial distribution of classification uncertainty (Dronova et al., 2011, 2012) as occurrence of objects with weak maximum class membership <0.5 as a potential indicator of previously unrecognized DCTs.

3. Results

3.1. Dominant spatial and temporal patterns revealed by EPCA

The T-mode EPCA results highlighted several temporally prevalent states of wetland surface that were largely consistent among NDVI, NDWI and ASAR series. The first component explained 94.7% variation in the data with high loading values from each date but especially October-late spring (Fig. 3a, Fig. 4a–c). For NDVI, this component highlighted differences in prevalence of green emergent vegetation (Fig. 4a), while for NDWI (Fig. 4b) and ASAR (Fig. 4c) series it reflected gradients of submersion time previously discussed by Andreoli et al. (2007) and Zhao et al. (2011). The second T-mode component (1.8%) accentuated differences between the higher flood stages in August and May and the low water season, especially January (Fig. 3a, Fig. 4d–f). For NDVI, this component contrasted emergent winter vegetation in the central wetland area and upland areas with low submersion times, particularly high-elevation sand dunes and C4 grass-dominated features (Fig. 4d). For NDWI, it highlighted a more general contrast between flood-prone central wetland area and the rest of the landscape (Fig. 4e), and for radar — areas of permanent water regardless of turbidity or WAM presence (Fig. 4f). The third T-mode component (1.2%) was much noisier than the first two, but consistent among NDVI and NDWI series, showing the contrast between early and late stages of the flood cycle (Fig. 3a); for radar, it also accentuated flood-free areas in winter. The remaining components were generally noisy and often redundant with the first three components or sensitive to patterns not relevant to DCTs, for instance, prevalence

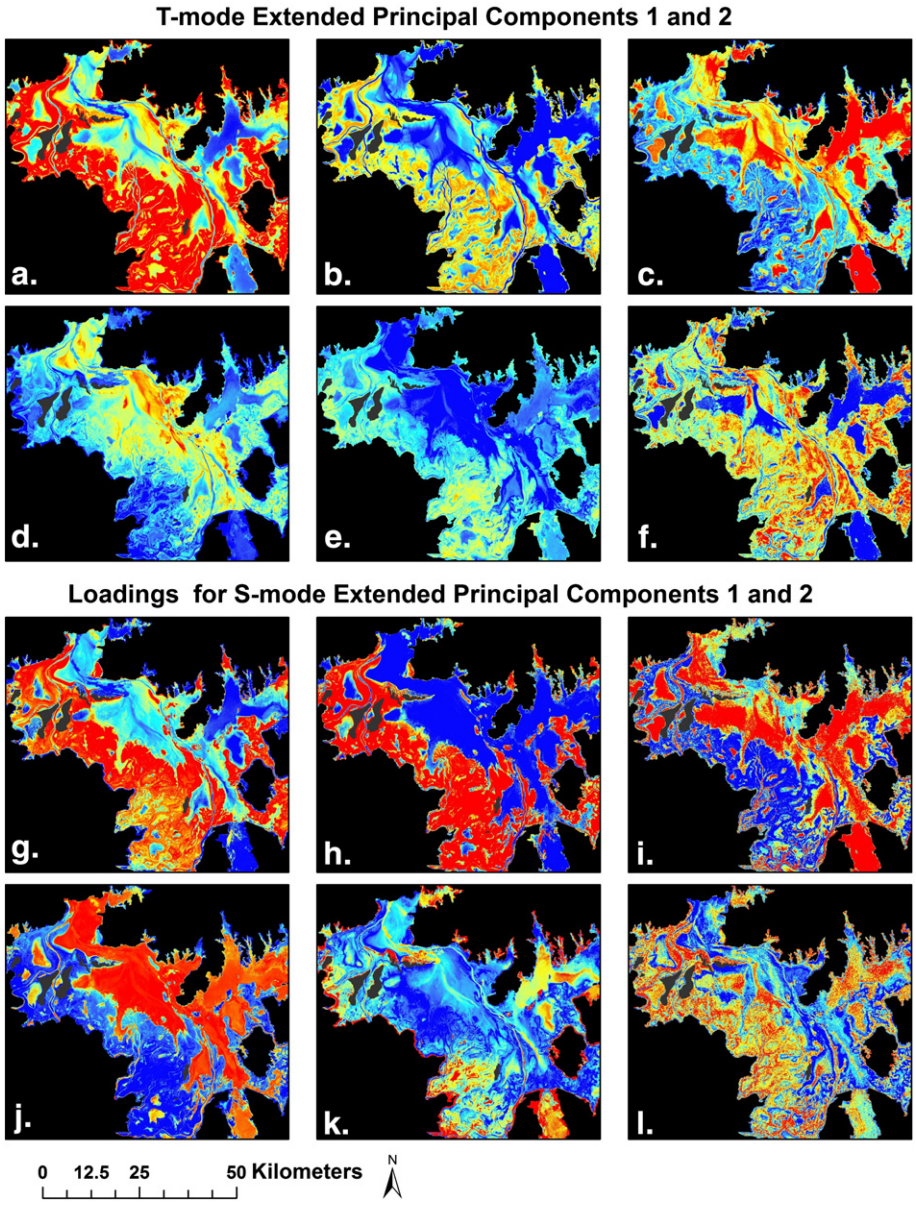

Fig. 4. Visualizations of the spatio-temporal patterns highlighted by EPCA for the major part of Poyang Lake area: a)–c) T-mode extended component1 for NDVI, NDWI and radar series, respectively; d)–f) T-mode extended component2 for NDVI, NDWI and radar series, respectively; g)–i) loading images for S-mode extended component 1 for NDVI, NDWI and radar series, respectively; and j)–l) loading images for S-mode component 2 for NDVI, NDWI and radar series.

of turbid water in some of the permanent water bodies from multi-spectral series. Among them, of particular interest was component 7 of NDVI and NDWI contrasting late fall and mid-winter (Fig. 3a) for areas where some of the ephemeral vegetation and WAM beds had developed.

The first component of the S-mode EPCA (37.7% variation) highlighted one of major Poyang Lake's temporal profiles — the overall change from August 2007 and late spring 2008, most pronounced between the first two and the last two image dates (Fig. 3b). For all three image series, this pattern matched the increase in greenness of emergent vegetation in more upland areas and contrasted with dynamics of permanent water and inundation-prone central wetland area (Fig. 4g–i). The second S-mode component explained comparable amount of variation (35.4%) and emphasized largely the change between mid-winter and late spring 2008 (Fig. 3b). This trajectory was manifested differently among three input series. For NDVI (Fig. 4j), it correlated most strongly with DCTs that gradually increased in greenness and stayed flood-free by late spring (C3 and mixed C3-C4 grasslands). For NDWI this trajectory matched features within minimal or no submersion at the highest flood stage (Fig. 4k). For radar data, it contrasted ephemeral vegetated and non-vegetated mudflats with permanent water, sand and grasslands (Fig. 4l). Component 3 (9.7% variation) represented trajectories with values increasing from August to October 2007, then decreasing to March–April and increasing again by late spring (Fig. 3b). This pattern, though noisier, correlated positively with mixed C3–C4 grasslands, and negatively — with some of the turbid water bodies and mudflats in NDVI and NDWI series. The other components were noisier and more difficult to match to specific DCTs (Fig. 3b).

3.2. Statistics of the training samples for input image series and EPCA results

Temporal profiles of class means from the training sample set showed unique change pathways for classes despite similarities in some of the states and transitions within their overall trajectories (Fig. 5). For the NDVI series, by the end of spring 2008 DCTs diverged into “greener” pathways dominated by emergent vegetation and

"wetter" flooded types (Fig. 5a). Trajectories of permanent sand and water features were largely invariant; some variation in water color occurred due to changes in lake turbidity.

The signal of class wetness in the NDWI series was inversely correlated with NDVI profiles (Fig. 5b) and largely mirrored them, also showing the largest divergence among classes in late spring. The backscatter time series were less effective in showing the differences among individual classes; however, they contrasted "upland" grasslands and sand dunes with lower-elevation ephemeral mudflats and permanent water (Fig. 5c).

Multiple comparisons with Scheffé's test detected statistically significant differences in mean training object EPCA output values for different pairs of classes. No single T- or S-mode component separated all 28 class pairs; however, 24–26 pairs were significantly different with the first three T-mode extended components for NDVI and NDWI and first T-mode component for radar (details in Table A1, Appendix). Some of the lower-variation components, such as T-mode EPCs 5 and 7 for NDWI, separated more than 20 class pairs. Several T- and S-mode components discriminated one or more individual DCTs from all the other classes (Table A1); of those, the first T-mode component for NDWI separated four wettest classes from each other and from upland grasses and sand. In addition to spectral values, some object-level textural metrics of standard deviation in component or loading images were effective in separating DCTs. Specifically, 21 and 22 class pairs were significantly different in S-mode loading values of NDVI components 1 and 3, respectively; both loading images also discriminated sand from other classes (Table A1). Overall, these results confirmed class differences evident from EPCA output images (Fig. 4) and suggested that a number of EPCA outputs were redundant in their ability to discriminate classes.

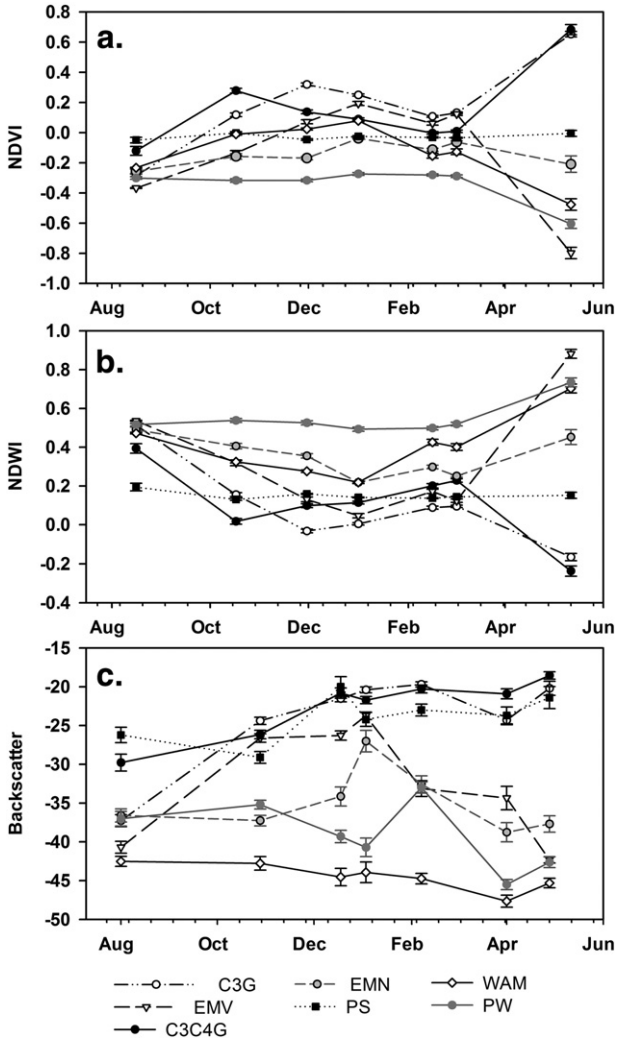

Fig. 5. Temporal trajectories of DCTs estimated as mean training object values of the non-transformed input layers from a) Beijing-1 NDVI, b) Beijing-1 NDWI and c) ASAR backscatter coefficient. Vertical error bars indicate standard error of the class mean.

3.3. Classification accuracy and DCT map for summer 2007–spring 2008 period

The highest classification accuracy was achieved with a larger set of 33 attributes (Table A2, Appendix) from combined time series and EPCA results (overall accuracy 95.0%, kappa 0.94, Table 3). Accuracies based on smaller variable sets from EPCA outputs or input images alone were comparably high (94.7% and 93.1, respectively, Table 3). Major sources of error were consistent among three attribute sets and included primarily the mutual confusion of emergent flooded C3 grassland and mixed C4-C3 grassland and misclassification of ephemeral non-vegetated mudflats mainly with vegetated mudflats, permanent water and WAM. The C3C4G class had generally lower user's and producer's accuracy than most other classes, likely due to inclusion of C3 grasses within C4 grass matrix (Dronova et al., 2012); its accuracy was improved by using EPCA outputs either alone or together with the input image data (Table 3). For EMN class, using EPCA attributes substantially increased user's accuracy, but at the same time reduced producer's accuracy, suggesting that other DCTs benefited more strongly from EPCA than did EMN. The map of the highest-accuracy DCT classification result (Fig. 6a) highlighted differences in DCT distributions based on their trajectories, where classes with shorter inundation stage occurred

Table 3
Contingency matrices for assessment of accuracy for dynamic cover type classification in summer 2007–spring 2008 flooding period based on three sets of attributes selected by machine-learning search.

Assigned class	Reference class							User's accuracy, %
	C3G	EMV	C3C4G	EMN	PS	WAM	PW	
Attributes: combined image and PCA, overall accuracy 95.0%, kappa 0.942%								
C3G	55	4						*93.2*
EMV	5	46		2				*86.8*
C3C4G			50					*100.0*
EMN				41				*100.0*
PS					40			*100.0*
WAM				2		50		*96.2*
PW				5			60	*92.3*
Producer's accuracy, %	*91. 7*	*92.0*	*100.0*	*82.0*	*100.0*	*100.0*	*100.0*	
Attributes: PCA-based inputs only, overall accuracy 94.7%, kappa 0.938								
C3G	54	2						*96.4*
EMV	6	47		2	2			*82.5*
C3C4G			50	2				*96.2*
EMN				42				*100.0*
PS		1		1	38			*95.0*
WAM				1		50		*98.0*
PW				2			60	*96.8*
Producer's accuracy, %	*90.0*	*94.0*	*100.0*	*84.0*	*95.0*	*100.0*	*100.0*	
Attributes: image series-based inputs only, overall accuracy 93.1%, kappa 0.920								
C3G	51	6						*89.5*
EMV	5	43		1	1			*86.0*
C3C4G			48					*100.0*
EMN	4		2	46			2	*85.2*
PS		1			39			*97.5*
WAM				1		50		*98.0*
PW				2			58	*96.7*
Producer's accuracy, %	*85.0*	*86.0*	*96.0*	*92.0*	*97.5*	*100.0*	*96.7*	

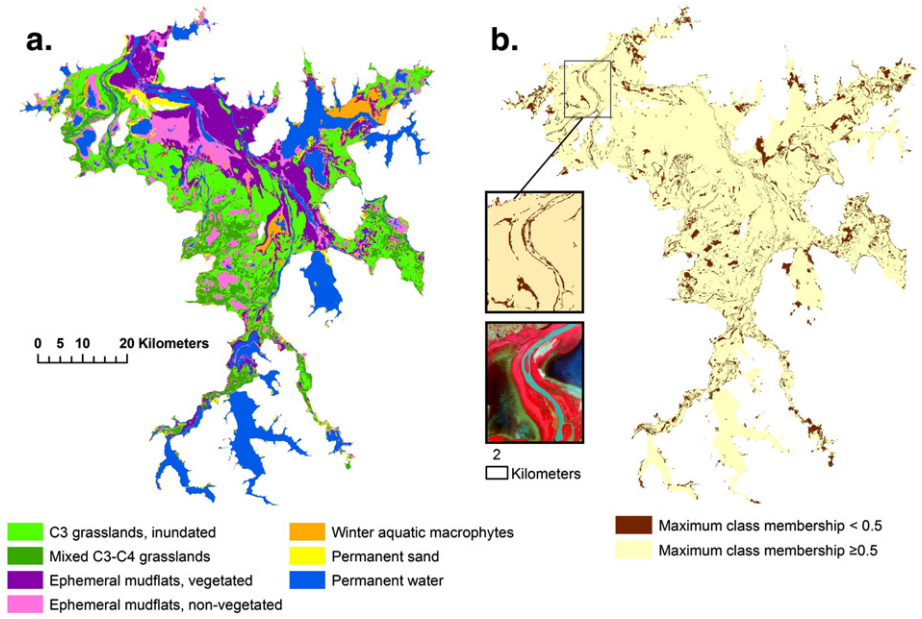

Fig. 6. Map of Poyang Lake's dynamic cover types (DCTs) for summer 2007–spring 2008 flood period based on the highest-accuracy classification result: a) spatial distribution of DCT classes and b) classification uncertainty expressed as locations with primary class membership < 0.5. Two insets show an enlarged portion of the study area corresponding to edge of a sub-lake with the river channel right from it and the corresponding view of the same area in the high-resolution QuickBird image from May 2007 displayed as near-infrared, red and green band composite.

closer to wetland periphery, while inundated vegetated and non-vegetated mudflats were adjacent to water bodies.

Areas with high classification uncertainty corresponding to objects with maximum class membership value <0.5 occupied ~8.6% of the study area and occurred primarily along mapped class boundaries (Fig. 6b). Some of these formed linear features corresponding to narrow rivers and channels that likely were not accurately represented at the 32 m resolution of the input data. Interestingly, some of the more extensive clusters of uncertain objects occurred at the interface of permanent water and non-vegetated mudflats, and their highest membership values were typically for EMN, PW or C3G. Closer investigation of a subset of these areas with available high-resolution images for May 2007 suggested that these were inundated mudflats and edges of water bodies with beds of aquatic vegetation in late spring. Due to the lack of reference ground data for these locations and limited field access to them at the high water stage, we were not able to differentiate emergent, floating and submerged macrophytes within these patches, nor to characterize them as a standalone DCT in this study. Mapping aquatic macrophytes at Poyang Lake is challenging in general (Wang et al., 2012) because of their localized distribution, complex patch structure, and also high water turbidity and frequent cloud cover in the warm growing season.

4. Discussion

4.1. The potential of dynamic object-based classifications to facilitate analyses of complex wetlands

It is increasingly recognized that efforts to understand ecological resilience and to facilitate planning, management and conservation of ecosystem services need to view landscapes as mosaics of nested regimes rather than simple static cover types (Lymburner et al., 2011; Parrott & Meyer, 2012; Watson et al., 2014). Areas with considerable short-term surface dynamics, such as periodically inundated wetlands, require special approaches for assessing their characteristic regimes and longer-term transitions (Crews-Meyer, 2008; Evans, Costa, Telmer and Silva, 2010; Hess et al., 2003 Lymburner et al., 2011). Multi-date remote sensing data are critical both for circumventing field observation challenges in wetlands and for providing temporal "context" to interpret surface features (Feng et al., 2012; Wang et al., 2012). Our results suggest that this potential of remote sensing can be further amplified by informing target change trajectories with prior environmental data, highlighting dominant states and transitions by EPCA of complementary image datasets and by incorporating spatial context of local dynamics using OBIA to alleviate the effects of local heterogeneity on classification outcomes.

In the complex Poyang Lake wetlands, process-based understanding of surface properties has to date been limited by large spatial extent, difficult field access and the lack of spatially and temporally comprehensive ground information. Using the dynamic cover type approach allowed us to characterize Poyang Lake area as a mosaic of change trajectories relevant to major surface features and cycles of vegetation phenology. High DCT classification accuracy achieved with different sets of discriminating spectral and textural attributes (Table 3) suggested that classes defined with prior information represented major change regimes in this wetland reasonably well. Their mapped distributions were consistent with previous analyses of Poyang Lake's hydrology and vegetation, reflecting gradients of submersion time (Andreoli et al., 2007; Hui et al., 2008; Zhao et al., 2011) and prevalence of green vegetation based on phenology of different plant functional types (Dronova et al., 2012; Wang et al., 2012). As with any remote sensing classification, however, definitions of dynamic classes depend on specific research objectives, and future work should test alternative class schemes and more specific change trajectories describing anthropogenic disturbance and habitats of endangered fauna.

Importantly, DCTs accentuated different "schedules" for compositionally similar classes with different roles in annual ecosystem dynamics. For example, late fall and early winter expansion of C3 grasses at Poyang Lake occurs both within peripheral wetlands (C3G) and near the central water body (EMN). Both classes may be spectrally similar on single-date images in winter due to growth of C3 grasses in EMN and grazing pressure on the established plants in C3G (Chen et al., 2007; Wang et al., 2012, Fig. 5a–c). However, at the seasonal and annual time scales, these DCTs are likely to contribute differently to ecosystem biogeochemical fluxes and habitats because of their unique schedules of vegetation emergence, peak density and biomass and the overall flood-

free time. Studies of greenhouse gas fluxes and nutrient cycling at Poyang Lake have not yet explicitly quantified components of flux source/sink dynamics (Liu et al., 2013), and understanding spatial distribution of plant phenological cycles would be a key step towards this knowledge. Previous efforts to detect and map ephemeral winter vegetation were challenged by temporal heterogeneity of its emergence in single-date images and the lack of field access to mudflats in the central wetland area (Liu, 2009). Considering distinct spatial and temporal features of EMV class with the DCT approach may thus be a useful strategy to facilitate its detection in the future.

Using object-based image analysis benefited DCT classification by smoothing the local spectral noise, taking advantage of object-level texture metrics and incorporating spatio-temporal context of pixels within small primitive objects, similar to previous studies (Bontemps, Bogaert, Titeux and Defourny, 2008; Conchedda et al., 2008; Desclée, Bogaert and Defourny, 2006; Stow, Hamada, Coulter and Anguelova, 2008). As noted earlier, pixel speckle may increase variation in class trajectories and obscure meaningful transitions (McCleary et al., 2008). This variation was addressed by integrating pixel values within small objects assumed to be spatially invariant multi-temporal DCT units during one flood cycle. This assumption was based on previous observations that major Poyang Lake vegetation and surface features form recognizable patches shaped by topography affecting local hydroperiod, ecological interactions of plant species and disturbance from inundation and grazing. Assuming invariant objects as units of multi-temporal landscape analysis was also useful in a number of other studies where spatial heterogeneity was attributed to natural surface complexity and/or high image resolution (e.g., Conchedda et al., 2008; Duveiller, Defourny, Desclee and Mayaux, 2008; Stow et al., 2008). However, over longer time scales, spatial properties and geometry of multi-temporal patches are likely to change, indicating potential expansions or contractions in landscape change regimes represented by dynamic classes. Thus, extension of DCT analyses to multiple flood cycle periods would require rigorous assessments of the "object fate" and dynamics of object boundaries (Niemeyer, Marpu and Nussbaum, 2008; Schoepfer, Lang and Albrecht, 2008).

4.2. Benefits of spatial and temporal PCA in DCT delineation

Using extended PCA (Neeti & Eastman, 2014) facilitated detection of dominant spatial and temporal patterns of wetland change from three input time series of greenness, wetness and radar backscatter. While a number of previous studies used PCA to detect specific types of change (e.g., Byrne et al., 1980; Collins & Woodcock, 1996; Ribed & Lopez, 1995; Villa, Boschetti, Morse and Politte, 2012), to date there have been very few comparisons of T-mode versus S-mode results in land cover change analysis (Machado-Machado et al., 2011; Neeti & Eastman, 2014). In our study, EPCA results for one flood cycle at Poyang Lake indicated that while both modes facilitated classification, the T-mode was especially effective in showing prevalence of high and low greenness states that differed between classes with similar trajectories, such as upland C3 grasses and short-term ephemeral vegetation. In several cases spatial patterns of T-mode PC values and S-mode loading coefficients were similar (Fig. 4), suggesting redundancy in patterns captured by each orientation, also discussed by Neeti and Eastman (2014). Here this redundancy could be attributed to synchrony in transitions from states occupying large portions of the study area and thus explaining large components of both spatial and temporal variation in the data — such as expansion of C3 grasses or decreasing extent of water coverage during flood recession.

Contrary to expectations, the S-mode components did not fully differentiate specific seasonal temporal trajectories among individual DCTs. Instead, the primary benefit of the S-mode EPCA was in highlighting dominant general schedules of landscape change that explained most variation in the spatio-temporal data and thus helped to discriminate broader groups of classes based on duration of submersion or high and low greenness states. For instance, the first and second extended S-mode components (Fig. 3b, Fig. 4g, j) highlighted similar magnitudes of change in greenness among locations with different start and end NDVI values. Such transitions may be difficult to identify from single-date images or T-mode decomposition alone because of spectral contrasts and phenological variation within vegetation patches; however, similarity in direction and magnitude of their change was captured by the S-mode patterns. At the same time, unique class trajectories were not explicitly captured by S-mode components, likely due to heterogeneity in pixel-level trajectories caused by atmospheric effects, noise, local topographic and phenological variation and non-hydrological disturbance such as grazing.

The latter issue also underscores the importance of using ancillary information to define and interpret multi-step change trajectories in complex landscapes. Completely unsupervised change analyses may be penalized by the uncertainty due to local variability in transitions from the same change regimes and detection of physically implausible pathways (McCleary et al., 2008). Furthermore, from the standpoint of landscape ecology and management, wetland areas with slightly different schedules may still belong to the same dynamic classes, or regimes. For instance, ephemeral mudflats exposed at different times of the low water season may all constitute critical habitat for wintering waterbirds that "track" mudflat availability (Canepuccia, Isacch, Gagliardini, Escalante and Iribarne, 2007; Roshier & Reid, 2002). Similarly, seasonal variation in turbidity of permanent water was captured by PCA, but was not relevant to our study as a standalone change type. For the latter reason, it was useful to incorporate radar data providing useful information on change in water extent not affected by signals of turbidity or submersed aquatic plants.

4.3. Study limitations and insights for future work

Limited availability of cloud-free remote sensing data for the study area affected the uncertainty in our analysis and DCT classification. One important caveat was the potential uncertainty of class boundaries dictated both by classifier performance and by spatial resolution and temporal frequency of the available data (Lunetta et al., 2004). Classes with the highest mutual confusion (Table 3) were often spatial neighbors (Fig. 6a), hence their boundaries were likely to contain "mixed objects" (Lyons et al., 2012) as also suggested by higher classification uncertainty along class edges (Fig. 6b). Some of the aquatic plant species contributing to this uncertainty provide critical food for endangered waterbirds in winter (Barzen et al., 2009), and comprehensive monitoring of these resources would ideally require higher-resolution data and bathymetric assessments in turbid waters. Misclassification could also occur because parts of temporal trajectories for some locations had been missing in the image series and thus not detected by the analysis. However, too frequent temporal representation may also increase classification uncertainty due to short-term noise and within-class temporal heterogeneity (Zhong et al., 2011). Thus, future work should test the effect of data frequency on DCT classification, potentially with more frequent time series such as daily or 8- and 16-day composites of Moderate Resolution Imaging Spectroradiometer (MODIS) and class definitions appropriate for its spatial resolution.

Another challenge in DCT analysis was potential pixel-level noise from atmospheric effects in Beijing-1 data and incongruity between complex structure of wetland cover and relatively coarse spatial resolutions of both remote sensing datasets. PCA results on radar data were frequently more speckled than multi-spectral even in the highest-variance components. This issue was partially alleviated by applying EPCA to both Beijing-1 and radar images, and by using OBIA which allows to smooth radar noise (e.g., Evans et al., 2010; Grenier et al., 2007) and to incorporate simple measures of class texture at the primitive object level. Importantly, in humid and cloudy wetland regions, such as the study area, radar data are highly valuable for terrain and surface water monitoring (Andreoli et al., 2007) and may greatly

complement sparser multi-spectral image series (Grenier et al., 2007). Future work should explore the potential to facilitate dynamic classifications of inundated areas by fusion of multi-spectral and higher-resolution radar time series.

Our results also suggest that the effect of selected attributes on performance of supervised classifiers should be investigated more in-depth in the future. Relatively large sets of attributes were selected for classification from input image series and EPCA outputs either alone or combined. This outcome was not surprising because by definition, DCTs shared some of the states and transitions within their trajectories and were likely to be confused under a limited set of discriminating variables. At the same time, high classification accuracy achieved with large number of attributes raises concerns about potential over-prediction of classes for a specific year or flood cycle when extending the trained algorithm to map dynamic classes over multiple change periods. This should be tested in the future with consistent image series across multiple change cycles. Relative utility of attribute selection methods (e.g., different algorithms within Weka (Witten & Frank, 2009), feature optimization tool in eCognition (ECognition Developer 8 Reference Book. V.8.8., 2012) and others) should also be assessed to guide future analyses.

Finally, in extending dynamic classifications to multiple years or change cycles, it is important to develop the capacity for detecting "novel" or sporadic transitions triggered by short-term disturbance, unprecedented shifts in climate and hydrology, human management and restoration activities, or alien species invasions (Neuenschwander & Crews, 2008; Watson et al., 2014). This task also requires specific strategies for validation, which is often a challenge in multi-temporal studies (Liu & Cai, 2011), particularly in complex and variable areas. New cost-effective approaches such as wireless sensor networks (Burgess, Kranz, Turner, Cardell-Oliver and Dawson, 2010; Gong, 2007) and continuous observation of phenology with in situ digital photographs (Sonnentag et al., 2012) may provide reference information on change in such landscapes.

5. Summary

Wetland landscapes with high short-term surface dynamics are difficult to characterize by traditional classification and change detection methods. These complex landscapes often nest change regimes representing unique ecosystem processes and phenology, yet detecting them may be difficult due to large number of pixel-level change pathways and uncertainty of transitional states of surface cover. Using a DCT approach, our study characterized major change trajectories driven by seasonal flood dynamics and vegetation phenology of a single flood cycle in a large, spatially and temporally heterogeneous Poyang Lake wetland. Detecting key states and transitions of wetland cover was facilitated by using T- and S-mode orientations of the EPCA to extract joint patterns of variation among complementary multi-spectral and radar image series. The primary benefit of the T-mode analysis was in highlighting prevalent states of wetland cover that constituted large components of the hypothesized DCT trajectories, even for classes with smaller spatial extent. In turn, the key contribution of the S-mode decomposition was to reveal the dominant temporal pathways of wetland change. Although these pathways matched only some, but not all, of the DCT class trajectories, they highlighted major locations and directions of change in multi-spectral and backscatter values and key differences among DCTs, thus facilitating their classification. The highest accuracy achieved with attributes from both the time series and EPCA outputs was only marginally higher than the accuracy based on a smaller set of EPCA-only inputs, suggesting that the latter provide a useful strategy to reduce the large number of discriminating variables of the original time series. Using temporally invariant primitive objects as mapping units instead of pixels allowed us to account for local spatial context and to moderate the effect of local pixel variation on classification uncertainty.

By representing landscape zones that are likely to exhibit similar change patterns within a single flood cycle, DCTs may offer useful strata for studies of ecological processes, habitats for wildlife and infectious disease agents (Seto et al., 2002a) and inputs for hydrological, biogeochemical and climatic models in the complex Poyang Lake landscape. Such process-based understanding is urgently needed to assess the response of Poyang Lake's ecosystems to climate change (Sun et al., 2014) and hydrological alterations following operation of Three Gorges Dam upstream and construction of local water control structures (Barzen et al., 2009). To further advance the understanding of the complex Poyang Lake wetland environment and its change, future efforts should 1) compare DCTs across multiple change periods and assessing their reference variation with temporally frequent data and 2) develop techniques to detect short-term changes induced by ecologically important but localized disturbance such as reed harvesting, grazing and aquaculture. Future analyses should also test sensitivity of DCT classification outcomes to temporal frequency, spatial resolution and spectral sensitivity of the available data, particularly in data-limited environments with frequent cloud cover. Finally, this approach can be tested in other seasonally inundated wetlands globally (e.g., the Pantanal wetlands, Florida Everglades, Okavango Delta) and non-wetland dynamic landscapes.

Acknowledgments

This research was supported by the National Aeronautics and Space Administration (NASA) Earth and Space Science student Fellowship (NNX09AO27H, 2009–2012) and the National High Technology Program of China (2013AA122804). We are also grateful to the State Key Laboratory of Remote Sensing Science (Beijing, China), Professor Shuhua Qi and the Key Lab of Poyang Lake Ecological Environment and Resource Development (Jiangxi Normal University, China). The study benefited from the support and services of the University of California, Berkeley's Geospatial Innovation Facility (gif.berkeley.edu). We also thank three anonymous reviewers for the useful feedback on this manuscript.

Appendix A

Table A1
Separation of DCT training samples based on one-way analysis of variance and Scheffé's post hoc test.

Input layer	Significantly different class pairs and groups ($p < 0.05$)	Classes significantly different from all other DCTs ($p < 0.05$)
Object-level means of the T-mode extended component values		
EPC 1, NDVI	All except C3G-C3C4G and EMV-EMN-WAM	PW, PS
EPC 1, NDWI	All except C3G-C3C4G and C3G-PS	EMV, EMN, WAM, PW
EPC 1, radar	All except C3G-C3C4G-PS and EMV-EMN	WAM, PW
EPC 2, NDVI	All except C3G-WAM and C3C4G-PW-PS	EPH, EMN
EPC 2, NDWI	All except C3G-PS, EMN-PW and PS-PW	C3C4G, WAM, EMV
EPC 2, radar	All except C3-EMV, C3C4G-EMN-PS and PW-WAM	–
EPC 3, NDVI	All except EMV-WAM, EMV-PW and EMN-PS	C3G, C3C4G
EPC 3, NDWI	All except EMV-PS, C3C4G-EMN and PW-WAM	C3G
EPC 4, NDWI	All except C3-EMV, C3C4G-WAM, EMN-PS-WAM and PW-PS	
EPC 5, NDWI	All except C3-EMV, C3C4G-PS-PW and EMN-PS	
EPC 7, NDWI	All except C3G-C3C4G-PS, EMV-WAM, EMN-PW and C3C4G-PW	

(continued on next page)

Table A1 *(continued)*

Input layer	Significantly different class pairs and groups ($p < 0.05$)	Classes significantly different from all other DCTs ($p < 0.05$)
Object-level means of the S-mode extended component loading values		
EPC1, NDVI	All except EMN-EMV-WAM, EMN-PW, PS-PW and PS-WAM	C3G, C3C4G
EPC1, NDWI	All except C3G-C3C4G, EMV-PW-WAM and EMN-PS	
EPC1, radar	All except EMV-EMN-PS and PW-WAM	C3G, C3C4G
EPC2, NDVI	All except EMV-PW-WAM;	C3G, C3C4G, EMN, PS
EPC2, NDWI	PS from C3G, EMV, EMN and WAM; C3C4G from C3G and WAM; PW from C3G, WAM, EMV and EMN	
EPC2, radar	All except C3G-C3C4G-PS-WAM, PW-EMN and PW-C3G	
EPC3, NDVI	All except EMV-EMN-PW and C3C4G-PS-WAM	C3G
EPC3, NDWI	All except C3G-WAM, C3G-PA, EMV-EMN, EMV-PW and PS-WAM	C3C4G
Object-level standard deviations (texture)		
S-mode EPC1 loadings, NDVI	All except C3G-C3C4G-EMV and PW-EMN-WAM	PS
S-mode EPC3 loadings, NDVI	All except C3G-C3C4G-EMV, EMN-WAM and EMN-PW	PS
T-mode EPC 7, NDVI	PW and WAM from all other classes (except each other)	
S-mode EPC2 loadings, radar	All except C3G-C3C4G-EMN-PW and PW-WAM	EMV, PS

Table A2
Object attributes selected for DCT discrimination by bi-directional machine-learning search algorithm in Weka software from three subsets of input variables.

Both EPCA and image series (33 attributes total)	EPCA only (21 attributes)	Image series only (21 attributes)
Object-level mean values		
T-mode EPC 2–5 and 7 for NDWI	T-mode EPC 1–5 and 7 for NDWI	NDVI for Aug, Oct and Nov 2007 and Jan 2008
	T-mode EPC 1,2 and 7 for NDVI	
T-mode EPC 1,2 and 7 for NDVI	S-mode EPC 1 and 3 loadings for NDWI	Seven NDWI layers
S-mode EPC 1 loadings for NDVI	S-mode EPC 1 and 3 for NDVI	Radar backscatter for July and Oct 2007, and Feb and late Apr 2008
	T-mode EPC 1 for radar backscatter	
S-mode EPC 3 loadings for NDWI	S-mode EPC 1 and 2 loadings for radar backscatter	
S-mode EPC 1 and 2 loadings for radar backscatter		
Seven NDWI layers		
Five NDVI layers (Aug, Oct and Nov 2007; Jan and Mar 2008)		
Radar backscatter for July 2007, Jan and February 2008		
Object-level standard deviation values		
T-mode EPC 3 for NDVI	T-mode EPC 7 for NDVI	NDWI for Aug 2007
T-mode EPC 4 for NDWI	T-mode EPC 7 for NDWI	NDVI for Feb 2008
Radar backscatter for Jan 2008	S-mode EPC 1 and 3 loadings for NDVI	Radar backscatter for Jan 2008
	S-mode EPC 2 for radar backscatter	

Table A2 *(continued)*

Both EPCA and image series (33 attributes total)	EPCA only (21 attributes)	Image series only (21 attributes)
Object-level statistics calculated from seven image dates		
Mean seven-date NDVI		Mean seven-date NDVI
		Seven-date standard deviation of NDWI
		Seven-date standard deviation of radar backscatter

References

Andreoli, R., Yesou, H., Li, J., Desnos, Y. L., Huang, S., & De Fraipont, P. (2007). Poyang Hu (Jiangxi Province, P.R. of China) area variations between January 2004 and June 2006 using ENVISAT low and medium resolution time series. *Geographic Information Sciences, 13*, 24–35.

Assendorp, D. (2010). *Classification of pattern and process in small-scale dynamic ecosystems; with cases in the Dutch coastal dunes.* PhD Dissertation. the Netherlands: University of Amsterdam (172 p.).

Baatz, M., & Schäpe, M. (2000). Multiresolution segmentation — An optimization approach for high-quality multi-scale image segmentation. In J. Strobl, T. Blaschke, & G. Griesebner (Eds.), *Angewandte Geographische Informations-Verarbeitung XII* (pp. 12–23). Karlsruhe: Wichmann Verlag.

Barzen, J., Engels, M., Burnham, J., Harris, J., & G. Wu. (2009). Phase 2 Report: Potential impacts of a water control structure on the abundance and distribution of wintering waterbirds at Poyang Lake. Unpublished report submitted to Hydro-ecology Institute of the Yangtze Water Resources Commission. International Crane Foundation, Baraboo.Wisconsin, USA. 54 p. http://www.savingcranes.org/images/stories/pdf/conservation/Phase%202%20Report_English.pdf.

Blaschke, T., Lang, S., Lorup, E., Strobl, J., & Zeil, P. (2000). Object-oriented image processing in an integrated GIS/remote sensing environment and perspectives for environmental applications. In A. Cremers, & K. Greve (Eds.), *Environmental information for planning, politics and the public, vol. 2.* (pp. 555–570). Marburg: Metropolis.

Bontemps, S., Bogaert, P., Titeux, N., & Defourny, P. (2008). An object-based change detection method accounting for temporal dependences in time series with medium to coarse spatial resolution. *Remote Sensing of Environment, 112*, 3181–3191.

Burgess, S. S. O., Kranz, M. L., Turner, N. E., Cardell-Oliver, R., & Dawson, T. E. (2010). Harnessing wireless sensor technologies to advance forest ecology and agricultural research. *Agricultural and Forest Meteorology, 150*, 30–37.

Byrne, G. F., Crapper, P. F., & Mayo, K. K. (1980). Monitoring land-cover change by principal component analysis of multitemporal Landsat data. *Remote Sensing of Environment, 10*, 175–184.

Canepuccia, A. D., Isacch, J. P., Gagliardini, D. A., Escalante, A. H., & Iribarne, O. O. (2007). Waterbird response to changes in habitat area and diversity generated by rainfall in a SW Atlantic coastal lagoon. *Waterbirds, 30*, 541–553.

Cattell, R. B., & Murphy, G. (1973). *Factor analysis: An introduction and manual for the psychologist and social scientist.* Westport, Conn: Greenwood Pr (462 p.).

Chen, G., Hay, G. J., Carvalho, L. M. T., & Wulder, M. A. (2012). Object-based change detection. *International Journal of Remote Sensing, 33*, 4434–4457.

Chen, S., Su, X., Fang, L., & Chen, L. (2007). Carex dynamics as an environmental indicator in the Poyang Lake wetland area: Remote sensing mapping and GIS analysis. *Annals of GIS, 13*, 44–50.

Collins, J. B., & Woodcock, C. E. (1996). An assessment of several linear change detection techniques for mapping forest mortality using multitemporal Landsat TM data. *Remote Sensing of Environment, 56*, 66–77.

Conchedda, G., Durieux, L., & Mayaux, P. (2008). An object-based method for mapping and change analysis in mangrove ecosystems. *ISPRS Journal of Photogrammetry and Remote Sensing, 63*, 578–589.

Coppin, P., Jonckheere, I., Nackaerts, K., Muys, B., & Lambin, E. (2004). Digital change detection methods in ecosystem monitoring: A review. *International Journal of Remote Sensing, 25*, 1565–1596.

Coppin, P., Nackaerts, K., Queen, L., & Brewer, H. (2001). Operational monitoring of green biomass change for forest management. *Photogrammetric Engineering and Remote Sensing, 67*, 603–611.

Crews-Meyer, K. A. (2008). Landscape dynamism: disentangling thematic versus structural change in northeast Thailand. In M. J. Hill, & R. J. Aspinall (Eds.), *Land use change: Science, policy and management* (pp. 99–118). CRC Press.

De Leeuw, J., Si, Y., Zeng, Y., Gang, L., Li, L., & Liu, Y. (2006). Mapping flood recessional grasslands grazed by overwintering geese: An application of multi-temporal remote sensing. *ISPRS Proceedings: Remote Sensing: From Pixels to Processes, 8–11 May 2006, Enschede, The Netherlands* (5 p.).

Desclée, B., Bogaert, P., & Defourny, P. (2006). Forest change detection by statistical object-based method. *Remote Sensing of Environment, 102*, 1–11.

Dronova, I., Gong, P., Clinton, N. E., Wang, L., Fu, W., Qi, S. H., & Liu, Y. (2012). Landscape analysis of wetland plant functional types: The effects of image segmentation scale, vegetation classes and classification methods. *Remote Sensing of Environment, 127*, 357–369.

Dronova, I., Gong, P., & Wang, L. (2011). Object-based analysis and change detection of major wetland cover types and their classification uncertainty during the low water period at Poyang Lake, China. *Remote Sensing of Environment*, *115*, 3220–3236.

Dudgeon, D., Arthington, A. H., Gessner, M. O., Kawabata, Z. I., Knowler, D. J., Leveque, C., Naiman, R. J., Prieur-Richard, A. H., Soto, D., Stiassny, M. L. J., & Sullivan, C. A. (2006). Freshwater biodiversity: Importance, threats, status and conservation challenges. *Biological Reviews*, *81*, 163–182.

Duveiller, G., Defourny, P., Desclee, B., & Mayaux, P. (2008). Deforestation in Central Africa: Estimates at regional, national and landscape levels by advanced processing of systematically-distributed Landsat extracts. *Remote Sensing of Environment*, *112*, 1969–1981.

ECognition developer 8 reference book. V.8.8. (2012). (448 p.).

Evans, T. L., Costa, M., Telmer, K., & Silva, T. S. F. (2010). Using ALOS/PALSAR and RADARSAT-2 to map land cover and seasonal inundation in the Brazilian Pantanal. *Ieee Journal of Selected Topics in Applied Earth Observations and Remote Sensing*, *3*, 560–575.

Feng, L., Hu, C. M., Chen, X. L., Cai, X. B., Tian, L. Q., & Gan, W. X. (2012). Assessment of inundation changes of Poyang Lake using MODIS observations between 2000 and 2010. *Remote Sensing of Environment*, *121*, 80–92.

Finlayson, M., Harris, J., McCartney, M., Young, L., & Chen, Zh. (2010). *Report on Ramsar visit to Poyang Lake Ramsar site, P.R. China 12–17 April 2010. Report prepared on behalf of the Secretariat of the Ramsar Convention* (34 p.).

Foley, J. A., DeFries, R., Asner, G. P., Barford, C., Bonan, G., Carpenter, S. R., Chapin, F. S., Coe, M. T., Daily, G. C., Gibbs, H. K., Helkowski, J. H., Holloway, T., Howard, E. A., Kucharik, C. J., Monfreda, C., Patz, J. A., Prentice, I. C., Ramankutty, N., & Snyder, P. K. (2005). Global consequences of land use. *Science*, *309*, 570–574.

Gibbs, J. P. (2000). Wetland loss and biodiversity conservation. *Conservation Biology*, *14*, 314–317.

Gong, P. (2007). Wireless sensor network as a new ground remote sensing technology for environmental monitoring. *Journal of Remote Sensing*, *11*, 545–551.

Gong, P., Niu, Z. G., Cheng, X. A., Zhao, K. Y., Zhou, D. M., Guo, J. H., Liang, L., Wang, X. F., Li, D. D., Huang, H. B., Wang, Y., Wang, K., Li, W. N., Wang, X. W., Ying, Q., Yang, Z. Z., Ye, Y. F., Li, Z., Zhuang, D. F., Chi, Y. B., Zhou, H. Z., & Yan, J. (2010). China's wetland change (1990–2000) determined by remote sensing. *Science China-Earth Sciences*, *53*, 1036–1042.

Gong, P., & Xu, B. (2003). Remote sensing of forests over time: change types, methods, and opportunities. In M. Woulder, & S. E. Franklin (Eds.), *Remote sensing of forest environments: Concepts and case studies* (pp. 301–333). Amsterdam, Netherlands: Kluwer Press.

Grenier, M., Demers, A. M., Labrecque, S., Benoit, M., Fournier, R. A., & Drolet, B. (2007). An object-based method to map wetland using RADARSAT-1 and Landsat ETM images: Test case on two sites in Quebec, Canada. *Canadian Journal of Remote Sensing*, *33*, S28–S45.

Guan, Y., Lin, W., Zhou, F., & Zeng, N. (2008). Monitoring dynamics of grassland vegetation in Poyang Lake National Nature Reserve, using MODIS imagery. *The International Archives of the Photogrammetry, Remote Sensing and Spatial Information Sciences*, *37*(Part B8), 1337–1342.

Guo, H., Hu, Q., Zhang, Q., & Feng, S. (2012). Effects of the Three Gorges Dam on Yangtze River flow and river interaction with Poyang Lake, China: 2003–2008. *Journal of Hydrology*, *416*, 19–27.

Hall, M. A. (1999). *Correlation-based feature subset selection for machine learning.* PhD Thesis, Hamilton, New Zealand: The University of Waikato (198 p.).

Hall, M. A., Frank, E., Holmes, G., Pfaringer, B., Reutemann, P., & Witten, I. H. (2009). The WEKA data mining software: An update; SIGKDD explorations, 11(1). http://www.cs.waikato.ac.nz/ml/weka

Hess, L. L., Melack, J. M., Novo, E. M. L. M., Barbosa, C. C. F., & Gastil, M. (2003). Dual-season mapping of wetland inundation and vegetation for the central Amazon basin. *Remote Sensing of Environment*, *87*, 404–428.

Hui, F. M., Xu, B., Huang, H. B., Yu, Q., & Gong, P. (2008). Modelling spatial-temporal change of Poyang Lake using multitemporal Landsat imagery. *International Journal of Remote Sensing*, *29*, 5767–5784.

Kim, M., Warner, T. A., Madden, M., & Atkinson, D. S. (2011). Multi-scale GEOBIA with very high spatial resolution digital aerial imagery: Scale, texture and image objects. *International Journal of Remote Sensing*, *32*, 2825–2850.

Lawrence, R. L., & Ripple, W. J. (1999). Calculating change curves for multitemporal satellite imagery: Mount St. Helens 1980–1995. *Remote Sensing of Environment*, *67*, 309–319.

Lenssen, J., Menting, F., van der Putten, W. H., & Blom, K. (1999). Control of plant species richness and zonation of functional groups along a freshwater flooding gradient. *Oikos*, *86*, 523–534.

Liu, M. (2009). *Monitoring ephemeral vegetation in Poyang Lake using MODIS Remote Sensing Images.* M.Sc. Thesis. The Netherlands: The International Institute for Geo-information Science and Earth Observation (65 p. www.itc.nl/library/papers_2009/msc/nrm/liu.pdf).

Liu, D., & Cai, S. (2011). A spatial–temporal modeling approach to reconstructing land-cover change trajectories from multi-temporal satellite imagery. *Annals of the Association of American Geographers*. http://dx.doi.org/10.1080/00045608.2011.596357.

Liu, L. X., Xu, M., Lin, M., & Zhang, X. (2013). Spatial variability of greenhouse gas effluxes and their controlling factors in the Poyang Lake in China. *Polish Journal of Environmental Studies*, *22*, 749–758.

Lu, D., Mausel, P., Brondizio, E., & Moran, E. (2004). Change detection techniques. *International Journal of Remote Sensing*, *25*, 2365–2407.

Lunetta, R. S., Johnson, D. M., Lyon, J. G., & Crotwell, J. (2004). Impacts of imagery temporal frequency on land-cover change detection monitoring. *Remote Sensing of Environment*, *89*, 444–454.

Lymburner, L., Tan, P., Mueller, N., Thackway, R., Thankappan, M., Islam, A., Lewis, A., Randall, L., & Senarath, U. (2011). The national dynamic land cover dataset — Technical report. *Record 2011/031*. Canberra: Geoscience Australia (http://www.ga.gov.au/metadata-gateway/metadata/record/71069/).

Lyons, M. B., Phinn, S. R., & Roelfsema, C. M. (2012). Long term land cover and seagrass mapping using Landsat and object-based image analysis from 1972 to 2010 in the coastal environment of South East Queensland, Australia. *ISPRS Journal of Photogrammetry and Remote Sensing*, *71*, 34–46.

Machado-Machado, E. A., Neeti, N., Eastman, J. R., & Chen, H. (2011). Implications of space–time orientation for principal components analysis of Earth observation image time series. *Earth Science Informatics*, *4*, 117–124.

Mas, J. F. (1999). Monitoring land-cover changes: a comparison of change detection techniques. *International Journal of Remote Sensing*, *20*, 139–152.

McCleary, A. L., Crews-Meyer, K. A., & Young, K. R. (2008). Refining forest classifications in the western Amazon using an intra-annual multitemporal approach. *International Journal of Remote Sensing*, *29*, 991–1006.

McFeeters, S. K. (1996). The use of the normalized difference water index (NDWI) in the delineation of open water features. *International Journal of Remote Sensing*, *17*, 1425–1432.

Mertens, B., & Lambin, E. F. (2000). Land-cover-change trajectories in southern Cameroon. *Annals of the Association of American Geographers*, *90*, 467–494.

Neeti, N., & Eastman, J. R. (2014). Novel approaches in extended principal component analysis to compare spatio-temporal patterns among multiple image time series. *Remote Sensing of Environment*, *148*, 84–96.

Neuenschwander, A. L., & Crews, K. A. (2008). Disturbance, management, and landscape dynamics: Harmonic regression of vegetation indices in the lower Okavango Delta, Botswana. *Photogrammetric Engineering and Remote Sensing*, *74*, 753–764.

Niemeyer, I., Marpu, P. R., & Nussbaum, S. (2008). Change detection using object features. In T. Blaschke, S. Lang, & G. Hay (Eds.), *Object-based image analysis spatial concepts for knowledge-driven remote sensing applications. Series: Lecture notes in geoinformation and cartography* (pp. 185–201). Berlin: Springer.

Ordoyne, C., & Friedl, M. A. (2008). Using MODIS data to characterize seasonal inundation patterns in the Florida Everglades. *Remote Sensing of Environment*, *112*, 4107–4119.

Ozesmi, S. L., & Bauer, M. E. (2002). Satellite remote sensing of wetlands. *Wetlands Ecology and Management*, *10*, 381–402.

Parrott, L., & Meyer, W. S. (2012). Future landscapes: Managing within complexity. *Frontiers in Ecology and the Environment*, *10*, 382–389.

Qi, S. H., Brown, D. G., Tian, Q., Jiang, L. G., Zhao, T. T., & Bergen, K. A. (2009). Inundation extent and flood frequency mapping using LANDSAT imagery and digital elevation models. *Giscience & Remote Sensing*, *46*, 101–127.

Rebelo, L. M., Finlayson, C. M., & Nagabhatla, N. (2009). Remote sensing and GIS for wetland inventory, mapping and change analysis. *Journal of Environmental Management*, *90*, 2144–2153.

Ribed, P. S., & Lopez, A. M. (1995). Monitoring burnt areas by principal components-analysis of multitemporal TM data. *International Journal of Remote Sensing*, *16*, 1577–1587.

Richman, M. B. (1986). Rotation of principal components. *Journal of Climatology*, *6*, 293–335.

Roshier, D. A., & Reid, J. R. W. (2002). Broad scale processes in dynamic landscapes and the paradox of large populations of desert waterbirds. *Avian Landscape Ecology: Pure and Applied Issues in the Large-Scale Ecology of Birds*, 148–155.

Schoepfer, E., Lang, S., & Albrecht, F. (2008). Object-fate analysis — Spatial relationships for the assessment of object transition and correspondence. In T. Blaschke, S. Lang, & G. Hay (Eds.), *Object-based image analysis — Spatial concepts for knowledge-driven remote sensing applications* (pp. 785–802). Berlin: Springer.

Seto, K. C., Woodcock, C. E., Song, C., Huang, X., Lu, J., & Kaufmann, R. K. (2002a). Monitoring land-use change in the Pearl River Delta using Landsat TM. *International Journal of Remote Sensing*, *23*, 1985–2004.

Seto, E., Xu, B., Liang, S., Gong, P., Wu, W. P., Davis, G., Qiu, D. C., Gu, X. G., & Spear, R. (2002b). The use of remote sensing for predictive modeling of schistosomiasis in China. *Photogrammetric Engineering and Remote Sensing*, *68*, 167–174.

Sonnentag, O., Hufkens, K., Teshera-Sterne, C., Young, A. M., Friedl, M., Braswell, B. H., Milliman, T., O'Keefe, J., & Richardson, A. D. (2012). Digital repeat photography for phenological research in forest ecosystems. *Agricultural and Forest Meteorology*, *152*, 159–177.

Stow, D., Hamada, Y., Coulter, L., & Anguelova, Z. (2008). Monitoring shrubland habitat changes through object-based change identification with airborne multispectral imagery. *Remote Sensing of Environment*, *112*, 1051–1061.

Sun, F., Zhao, Y., Gong, P., Ma, R., & Dai, Y. (2014). Monitoring dynamic changes of global land cover types: Fluctuations of major lakes in China every 8 days during 2000–2010. *Chinese Science Bulletin*, *59*, 171–189.

Vågen, T. G. (2006). Remote sensing of complex land use change trajectories — A case study from the highlands of Madagascar. *Agriculture, Ecosystems & Environment*, *115*, 219–228.

Villa, P., Boschetti, M., Morse, J. L., & Politte, N. (2012). A multitemporal analysis of tsunami impact on coastal vegetation using remote sensing: A case study on Koh Phra Thong Island, Thailand. *Natural Hazards*, *64*, 667–689.

Wang, L., Dronova, I., Gong, P., Yang, W. B., Li, Y. R., & Liu, Q. (2012). A new time series vegetation–water index of phenological–hydrological trait across species and functional types for Poyang Lake wetland ecosystem. *Remote Sensing of Environment*, *125*, 49–63.

Watson, S. J., Luck, G. W., Spooner, P. G., & Watson, D. M. (2014). Land-use change: Incorporating the frequency, sequence, time span, and magnitude of changes into ecological research. *Frontiers in Ecology and the Environment*, *12*, 241–249.

Witten, I. H., & Frank, E. (2009). *Data mining: Practical machine learning tools and techniques* (2nd ed.). Amsterdam, the Netherlands: Morgan Kaufmann Publishers/Elsevier (525 p.).

Zeng, Y., Liu, Y., Liu, Y., & de Leeuw, J. (2007). Mapping grass communities based on multi-temporal Landsat TM imagery and environmental variables. In Weimin Ju, & Shuhe Zhao (Eds.), *Geoinformatics 2007: Remotely sensed data and information. Proceedings of SPIE, Vol. 6752*, (67521 K-1).

Zhao, X., Stein, A., & Chen, X. L. (2011). Monitoring the dynamics of wetland inundation by random sets on multi-temporal images. *Remote Sensing of Environment, 115*, 2390–2401.

Zhong, L. H., Hawkins, T., Biging, G. S., & Gong, P. (2011). A phenology-based approach to map crop types in the San Joaquin Valley, California. *International Journal of Remote Sensing, 32*, 7777–7804.